Study of image characteristics on digital image correlation error assessment

Marina Fazzini, Sébastien Mistou, Olivier Dalverny, Laurent Robert

Study of image characteristics on digital image correlation error assessment

M. Fazzini [a,*], S. Mistou [a], O. Dalverny [a], L. Robert [b]

[a] Ecole Nationale d'Ingenieurs de Tarbes, LGP, 47 avenue d'Azereix, 65016 Tarbes, France
[b] Ecole Mines Albi, CROMeP, Campus Jarlard, 81013 Albi, France

A B S T R A C T

In this paper, errors related to digital image correlation (DIC) technique applied to measurements of displacements are estimated. This work is based on the generation of synthetic images representative of real speckle patterns. With these images, various parameters are treated in order to determine their impact on the measurement error. These parameters are related to the type of deformation imposed on the speckle, the speckle itself (encoding of the image and image saturation) or the software (subset size).

Keywords:
Digital image correlation
Error assessment
Saturation
Encoding

1. Introduction

Digital image correlation (DIC) is an optical full-field measurement technique that was appeared twenty years ago [1–3]. It consists in recording with a camera some digital images of a specimen undergoing an in-plane displacement field and computing the image correlation by appropriate software. It is among the most popular optical methods, but it still suffers from a lack of characterization. In this way, very few studies have been conducted.

The parameters tested in this investigations are, for example, the speckle pattern [4–7], the subset size [4,6,8,9] or the subset shape function [9,10] .

Recently, systematic studies have been proposed by the French CNRS research network 2519 based on synthetic images undergoing a sinusoidal displacement field [11–14]. These results focus on the effect of parameters that have to be set in a DIC measurement relative to the software, namely subset size, shape function order and image interpolation. In this paper, we are going to study the parameters in relation with the encoding of the image: differences between series of 4-bit, 6-bit or 8-bit images (simulate images with high gradients of grey levels) and image saturation (simulate overexposed images), based on images similar to those used by the CNRS research network 2519.

2. Digital image correlation shape function in Aramis 2D [15]

Digital image correlation allows the measurement of displacement fields of a planar surface; a single camera acquires a sequence of images of a planar object under plane strain. Displacements of points distributed over the surface of the object are calculated from the grey-level analysis of the images [2]. Given two images corresponding to two deformation states of an object, to determine the correspondent of a point and its signature of the first image in the second, a similarity function is used. In practice, a single grey-level value is not the unique signature of a point, hence neighbouring pixels are used. From its principle, the image correlation technique can work correctly only with objects having a surface with a sufficiently random texture.

Let $f(\underline{x})$ and $g(\underline{x})$ be the grey levels in the reference and deformed images, respectively of a same material point, and let $\underline{x}=(x,y)$ and $\underline{X}=(X,Y)$ be the corresponding coordinate vectors. The unknown apparent 2D mechanical transformation Φ_M is such that $\boldsymbol{\Phi}_M(\underline{x})=\underline{X}$. Perfect advection of the texture would ensure the conservation relation:

$$g(\boldsymbol{\Phi}_M(\underline{x}))=f(\underline{x}) \tag{1}$$

This mechanical transformation Φ_M can be locally approximate by a shape function Φ because the correlation domains (D) are small. Let $\underline{x}_{\underline{0}=(u_0,v_0)}$ be a point in the centre of the subset D in the reference image, and let $\underline{x}=(u, v)$ an another point in this subset. In this point $\underline{x}$, the mechanical transformation is defined by:

$$\underline{X}=\boldsymbol{\Phi}_M(\underline{x})\approx\boldsymbol{\Phi}(\underline{x})=\underline{x}+\boldsymbol{\Psi}(\underline{x}) \tag{2}$$

where $\Psi(\underline{x})$ is the displacement in the point $\underline{x}$. With a Taylor expansion of this displacement $\Psi(\underline{x})$ about the centre $\underline{x_0}$ of the subset D, we can write:

$$\boldsymbol{\Phi}(\underline{x})=\underline{x}+\boldsymbol{\Psi}(\underline{x_0})+\frac{\partial\boldsymbol{\Psi}}{\partial\underline{x}}(\underline{x_0})(\underline{x}-\underline{x_0})+\frac{1}{2}(\underline{x}-\underline{x_0})^T\frac{\partial^2\boldsymbol{\Psi}}{\partial\underline{x}^2}(\underline{x_0})(\underline{x}-\underline{x_0})+\ldots \tag{3}$$

* Corresponding author. Tel.: +33 5 62 44 50 80; fax: +33 5 62 44 27 08.
E-mail address: marina.fazzini@enit.fr (M. Fazzini).

doi:10.1016/j.optlaseng.2009.10.012

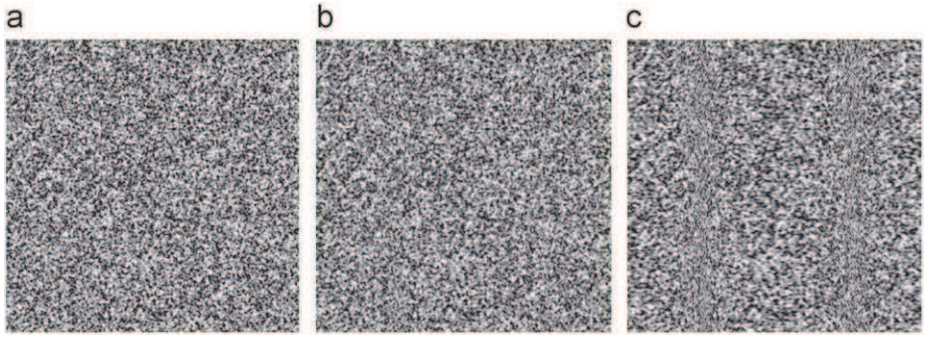

Fig. 1. Example of simulated synthetic images: reference (a) and deformed images (p=260 pixels, (b) α=0.02, (c) α=0.1).

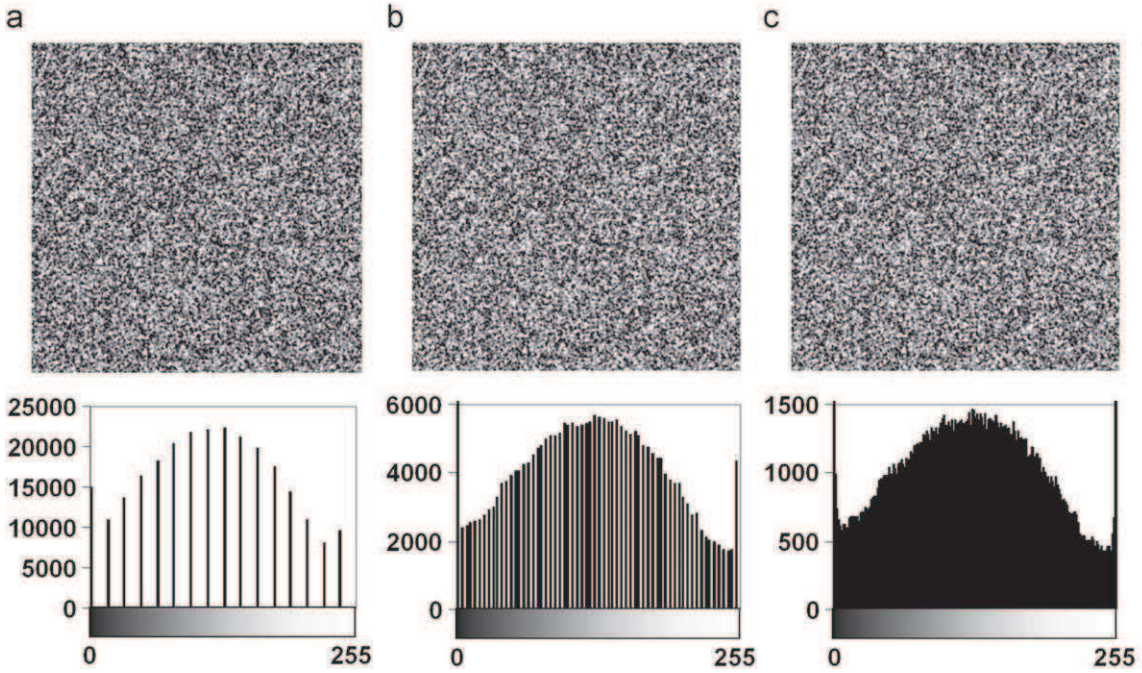

Fig. 2. 4-bit (a), 6-bit (b) and 8-bit (bit) reference images and grey-level histogram.

Truncation at various orders leads to different shape functions for the displacement field components along horizontal and vertical axes, respectively in the subset. Zero-, first- and second-order shape functions have already been tested in the work of the French CNRS research network 2519 [14]. In this study, the DIC software used (Aramis 2D®[15]) provides a first-order shape function that corresponds to the following bilinear transformation:

$$\boldsymbol{\Phi}(\underline{x}) = \begin{pmatrix} a_1 + a_2(x-x_0) + a_3(y-y_0) + a_4(x-x_0)(y-y_0) \\ a_5 + a_6(x-x_0) + a_7(y-y_0) + a_8(x-x_0)(y-y_0) \end{pmatrix} \quad (4)$$

The values a_1 and a_5 describe the translation of the facet's centre; the others describe the rotation and the deformation of the facet.

Then, the general algorithm consists in determining these parameters (a_i) by minimizing a correlation coefficient $C(\Phi)$, which measures the disparity between the grey-level distribution over the domain D in the reference image and the distribution over the deformed image back converted to the reference image according to Φ, as

$$\boldsymbol{\Phi}_D \approx \underset{\boldsymbol{\Phi} \in D}{\operatorname{Arg\,min}}\, C(\boldsymbol{\Phi}) \quad (5)$$

The correlation coefficient used by Aramis 2D® reads:

$$C(\boldsymbol{\Phi}) = 1 - \frac{\int_D (f(\underline{x_i}) - \overline{f})(g(\boldsymbol{\Phi}(\underline{x_i})) - \overline{g})dx}{\sqrt{\int_D (f(\underline{x_i}) - \overline{f})^2 dx}\sqrt{\int_D (g(\boldsymbol{\Phi}(\underline{x_i})) - \overline{g})^2 dx}} \quad (6)$$

with $\overline{f} = \int_D f(\underline{x})dx$

3. Results analyses procedure

As for the work of the French CNRS research network 2519 previously discussed, the sets of synthetic speckle-pattern images are obtained using the TexGen software [16]. These images are generated with a continuous noise function created from a Perlin's coherent noise. This function allows you to simulate a speckle pattern as realistic as possible spread over 256 grey levels with control of the speckle size, which produces synthetic 8-bit speckle-pattern images as realistic as possible to DIC speckle patterns. The set of deformed images is obtained assuming only an unidirectional sinusoidal displacement, which is given by

$$\underline{U}(\underline{x}) = \alpha p \sin\left(\frac{2\pi x}{p}\right)\underline{e_x} \quad (7)$$

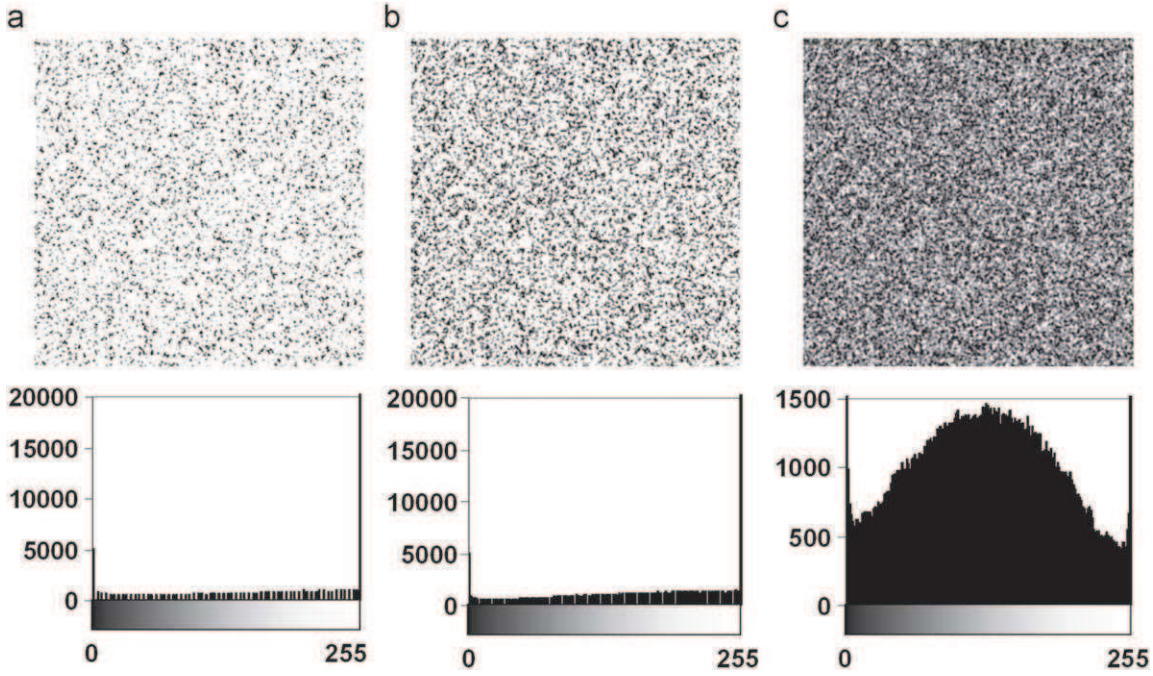

Fig. 3. Reference images for the 3 sets and grey-level histogram. (a) high saturated set, (b) saturated set and (c) standard set).

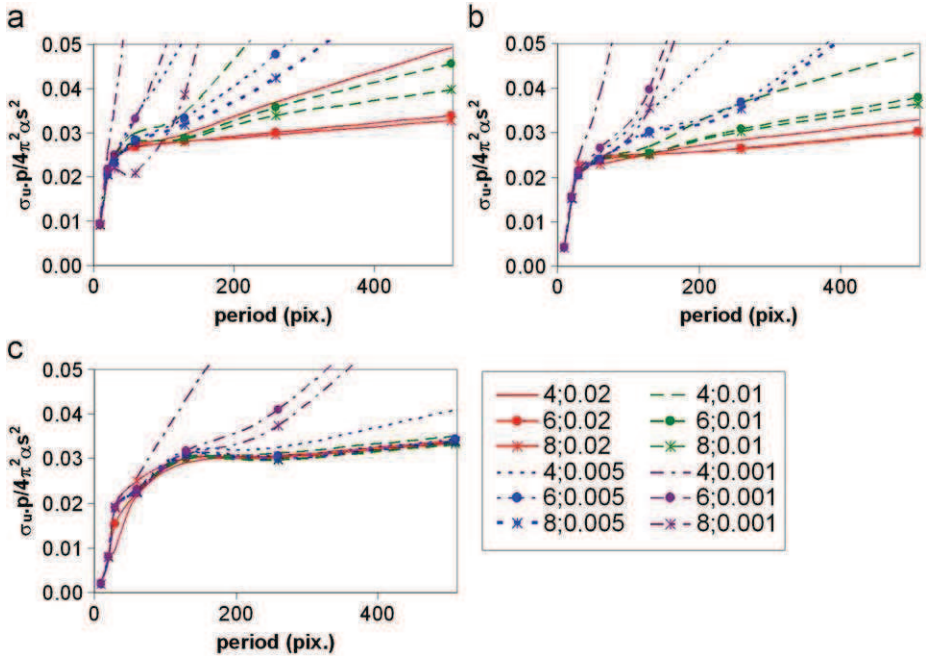

Fig. 4. Standard deviation of the displacement errors normalized by $4\pi^2\alpha s^2/p$ as a function of period p for various strain amplitudes α. Subset size s is equal to (a) 15, (b) 21 and (c) 31 pixels respectively (4-bit, 6-bit and 8-bit).

$$\underline{U}_{,x}(\underline{x}) = 2\pi\alpha\cos\left(\frac{2\pi x}{p}\right)\underline{e}_x = \underline{U}_{,x}^{\max}\cos\left(\frac{2\pi x}{p}\right)\underline{e}_x \tag{8}$$

$$\underline{U}_{,xx}(\underline{x}) = \frac{-4\pi^2\alpha}{p}\sin\left(\frac{2\pi x}{p}\right)\underline{e}_x = -\underline{U}_{,xx}^{\max}\cos\left(\frac{2\pi x}{p}\right)\underline{e}_x \tag{9}$$

where p is the period in pixel and αp the amplitude. Chosen values for the amplitude α and for the period p are $\alpha \in \{0.02, 0.01, 0.005, 0.001\}$ and $p \in \{10, 20, 30, 60, 130, 260, 510\}$ pixels, respectively for 512×512 pixel images. Note that corresponding values of the maximum strain are 12.6%, 6.3%, 3.1% and 0.6%. Fig. 1 shows some examples of both reference and deformed images. They are obtained for p=260 pixels and α=0.1 ($\underline{U}_{,x}^{\max}$=62.8%) and 0.02 ($\underline{U}_{,x}^{\max}$=12.6%).

A reference set is created with a grey-level histogram adjusted to obtain a broad distribution covering all 256 grey levels (Fig. 2(c) and Fig. 3(c)) and an autocorrelation radius *of* 2.2 pixels, radius at half height of the normalized autocorrelation function of the reference image, generally admitted as a value of the mean speckle grain size. As a first step, 4- and 6-bit like images are created. Aramis 2D® software uses only 8-bit images; that is why 16 grey levels of the 4-bit images and 64 grey levels of the 6-bit images vary between 0 and 255 (Fig. 2(a) and (b). This set simulates images more or less contrasted.

In a second stage, images simulating some more or less important light saturation generated by multiplying each pixel of each image of the reference set (reference and deformed images) by a factor of 2 (Figs. 3(b)) or 4 (Fig. 3(a)), values upper than 255 are set to the 255 level.

4. Results

Displacements are calculated at all locations of a regular square grid defined in the initial image, with pitches (sx; sy) such that subsets at adjacent positions do not overlap, thus ensuring the statistical independence of the corresponding errors. In practice sx=sy=s+1, where s is the subset size.

Square subsets of different sizes s are used, namely, 15, 21 and 31 pixels. Measured displacements U_{mes} are compared to imposed displacements U_{th} located at the centre of the subsets. The standard deviation σ_U of displacement errors (U_{mes}–U_{th}) at the centre of a subset is calculated as

$$\sigma_U = \sqrt{\frac{n\sum (U_{mes}-U_{th})^2 - (\sum (U_{mes}-U_{th}))^2}{n(n-1)}} \tag{10}$$

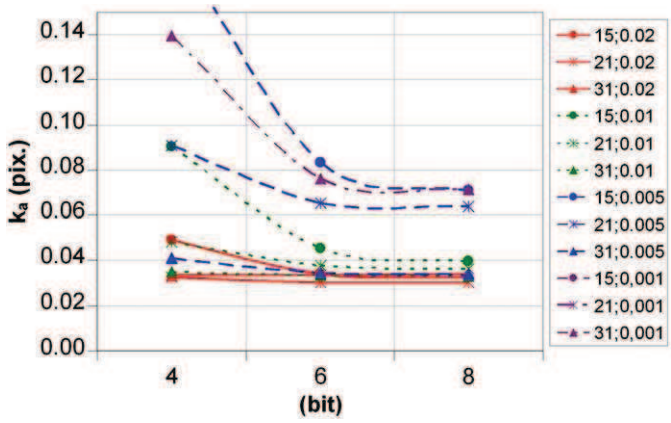

Fig. 5. Comparison of the asymptotic standard deviation of the displacement errors normalized by $4\pi^2\alpha s^2/p$ as a function of the type of image.

Fig. 4 shows the standard deviation normalized by a factor proportional to the square of the subset size and to the maximum second gradient of the displacement as a function of period p for 4-, 6- and 8-bit images. It has been shown in [11–14] that these curves can be analysed considering three zones. In the first one for small periods (typically for $p \le s$), the software evaluate nothing else than the standard deviation of the displacement itself. When the period is greater than about 5 s, an asymptotic value k_a can be reached. This asymptotic value is independent of α and s and is around 0.03. The second zone is the transition zone between the other two. However, it has been shown that for small subset and small strains, asymptotic value is not reached and is independent on p and α.

It is clearly seen that a decrease in the encoding deteriorates the measurement. Fig. 5 shows that the asymptotic value k_a of 6-bit like image results are upper but close to 8-bit image results, and 4-bit like image results are bad (except for the largest subset). For subset sizes of 15 or 21 pixels, the error value for large period (smallest strain gradient) is clearly dependant on the dynamic of images. Indeed, k_a values for 8-bit images are lower than k_a values for 4-bit images. When a larger subset size is considered, k_a values are much closer and the coding influence becomes negligible. As there is less information in 4-bit like images than in 8-bit images, for a giving error it needs a larger subset size that decreases the spatial resolution.

Fig. 6 shows the standard deviation normalized by a factor proportional to the square of the subset size and to the maximum second gradient of the displacement as a function of period p for the reference image set and for image set where each pixel of each image of the reference set is multiplied by a factor of 2 or 4 and limited to 255 grey level (saturated images). In this case, an asymptotic value k_a is never reached with the smallest subset size (Fig. 7). In fact, when the image is very exposed to light, size of the

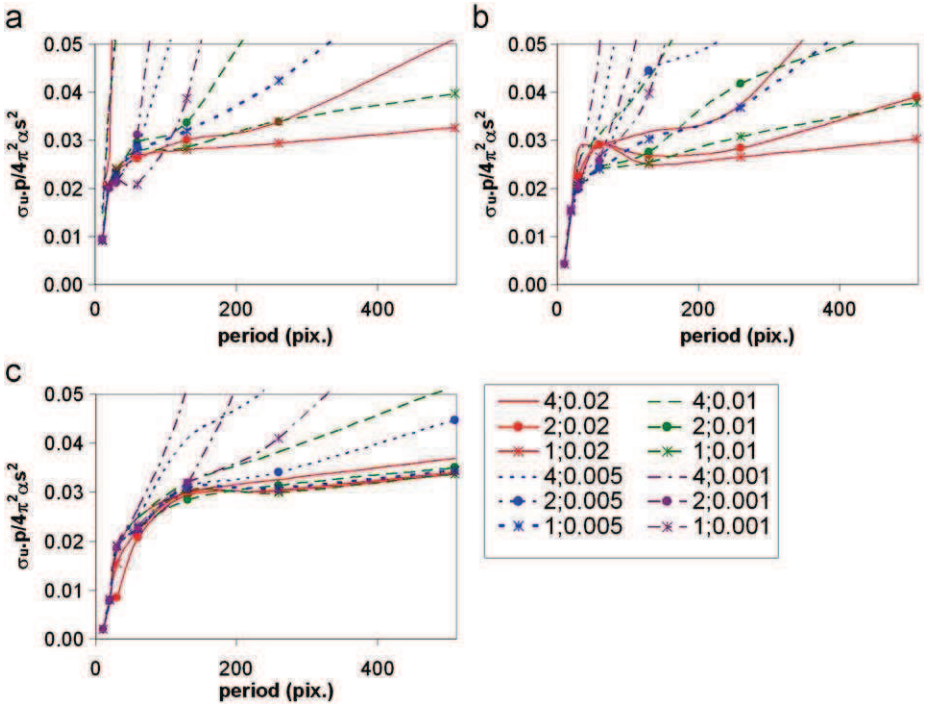

Fig. 6. Standard deviation normalized by $4\pi^2\alpha/p$ as a function of period p for various strain amplitudes α. Subset size s is equal to (a) 15, (b) 21 and (c) 31 pixels (saturation).

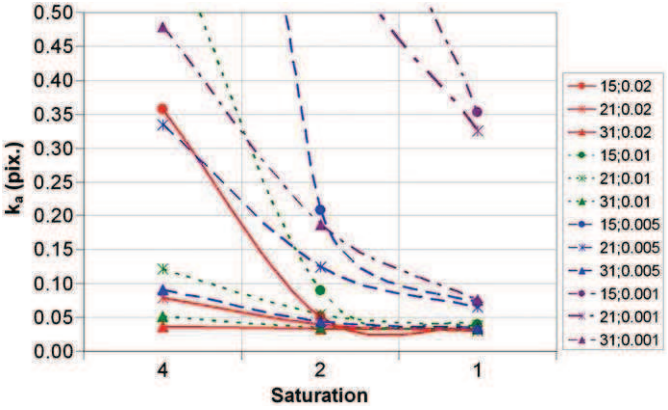

Fig. 7. Comparison of the asymptotic standard deviation of the displacement errors normalized by $4\pi^2\alpha s^2/p$ as a function of saturation.

white speckle grains increases (level 255) as size of the speckle grains of other grey level decreases. This results to images composed of small black patterns and large white patterns. Image correlation cannot work in this case if small subset size is used. The small subset/small amplitude effect previously seen in the Fig. 4 becomes more important with saturated images and can be found also with the larger subset. It is necessary, in this case too, to use subset sizes much more important to get an asymptotic value, but which worked in a more important error due to the subset size itself.

5. Conclusion

The aim of this work is to characterize the software in order to facilitate its use. Thus, different controllable parameters in a conventional use of the system (i.e. on real images captured with CCD) have been tested here. By creating well-controlled synthetic images, we are able to vary some parameters such as the type of encoding (4-, 6- or 8-bits) and the saturation independently. The DIC software treatment has been realised with different subset sizes, in order to highlight the relationship between image parameters and the DIC software parameters. With deformed images obtained assuming a unidirectional sinusoidal displacement with different values for the amplitude and the period, we created a set of images with a strong gradient of grey level (for 4- and 6-bit like images) and a set of images that simulates overexposed speckle. The results of the first set show that a decrease in encoding deteriorates the measurement by 2. The results of the second set show that an overexpose of the speckle deteriorates the measurement by 10.

Acknowledgements

This work was performed within the French CNRS research network 2519 "Full field measurement and identification in solid mechanics".

References

[1] Peters W, Ranson W. Digital imaging techniques in experimental stress analysis. Opt. Eng. 1982;21(3):427–31.
[2] Sutton M, Wolters W, Peters W, McNeill S. Determination of displacements using an improved digital correlation method. Image Vision Comput. 1983;1:133–9.
[3] Sutton M, McNeill S, Helm JD, Chao YJ. Advances in two-dimensional and three-dimensional computer vision. In: Rastogi PK, editor. Photomechanics. Berlin, Germany: Springer; 2000.
[4] Lecompte D, Smits A, Bossuyt S, Sol H, Vantomme J, Hemelrijck DV, Habraken A. Quality assessment of speckle patterns for digital image correlation. Opt. Lasers Eng. 2006;44:1132–45.
[5] Triconnet K, Derrien K, Hild F, Baptiste D. Parameter choice for optimized digital image correlation. Opt. Lasers Eng. 2009;47:728–37.
[6] Haddadi H, Belhabib S. Use of rigid-body motion for the investigation and estimation of the measurement errors related to digital image correlation technique. Opt. Lasers Eng. 2008;46:185–96.
[7] Pan B, Lu X, Xie H. Mean intensity gradient: an effective global parameter for quality assessment of the speckle patterns used in digital image correlation. Opt. Lasers Eng., in press, 2009, doi:10.1016/j.optlaseng.2009.08.010.
[8] Yaofeng S, Pang JH. Study of optimal subset size in digital image correlation of speckle pattern images. Opt. Lasers Eng. 2007;45:967–74.
[9] Lava P, Cooreman S, Coppieters S, De Strycker M, Debruyne D. Assessment of measuring errors in DIC using deformation fields generated by plastic FEA. Opt. Lasers Eng. 2009;47(7–8):747–53.
[10] Schreier H, Sutton M. Systematic errors in digital image correlation due to undermatched subset shape functions. Exp. Mech. 2002;42:303–10.
[11] Bornert M. Resolution and spatial resolution of digital image correlation techniques. Photomechanics. France: Clermont-Ferrand; 2006.
[12] Orteu J.-J. and Robert L., Estimation of digital image correlation (DIC) performances, International Conference on Experimental Mechanics (ICEM'13), Alexandroupolis (Greece), 1–6 July 2007.
[13] Orteu J.-J., Digital Image Correlation (DIC) Error Assessment, SEM Conference on Experimental and Applied Mechanics, Springfield, Massachusetts, USA, 4–6 June 2007.
[14] Bornert M, Brémand F, Doumalin P, Dupré JC, Fazzini M, Grédiac M, et al. Assessment of digital image correlation software packages. Exp. Mech. 2009;49(3):353-70.
[15] Aramis 2D® software. GOM-Gesellschaft für Optische Messtechnik mbH, Optical Measuring Techniques, http://www.gom.com/EN/index.html.
[16] Orteu J.-J., Garcia D., Robert L., and Bugarin F. (2006) A speckle-texture image generator. Proceedings of the Speckle'06 international conference, Nîmes, France.